Since January 2020 Elsevier has created a COVID-19 resource centre with free information in English and Mandarin on the novel coronavirus COVID-19. The COVID-19 resource centre is hosted on Elsevier Connect, the company's public news and information website.

CHAPTER

Nanoparticles: synthesis and applications

7

Nguyen Hoang Nam[1,2] and Nguyen Hoang Luong[2]

[1]Faculty of Physics, Hanoi University of Science, Vietnam National University, Hanoi, Hanoi, Vietnam [2]Nano and Energy Center, Hanoi University of Science, Vietnam National University, Hanoi, Hanoi, Vietnam

7.1 INTRODUCTION

Nanoparticles are defined by the worldwide federation of national standards bodies, the International Organization for Standardization (ISO), as nanoobjects with all external dimensions in the nanoscale, where the lengths of the longest and shortest axes of nanoobjects do not differ significantly (ISO/TS 80004-2:2015). Though nanoscale is basically ranged from 1 to 100 nm, nanoparticles can be categorized by three size ranges: larger than 500 nm, between 100 and 500 nm, and between 1 and 100 nm (European Commission, 2010). With respect to the size and the size distribution, nanoparticles may exhibit size-related intensive properties. If they are small enough to confine their electrons, they produce quantum effects and exhibit unexpected properties, for example, gold nanoparticles appear red in solution (see, for instance, Eustis and El-Sayed, 2006), and melt at much lower temperatures than that in slab form (Buffat and Borel, 1976). The high surface-area-to-volume ratio of nanoparticles provides the significant changes in properties related to contact/surface area, such as catalytic (Astruc, 2008), surface-enhanced plasmon resonance (Melaine et al., 2015), etc. Depending on the composition and structure, nanoparticles can be of single properties such as metallic, dielectric, semiconductor, magnetic, or multifunctional which include more than one feature from single-property nanoparticles. Their applications, or potential applications, are in many different fields (Salata, 2004; Mody et al., 2010; Lu et al., 2007; Zhang et al., 2008; Nguyen et al., 2015; and references therein). Among those, the advantages of nanoparticles in applications in life sciences and the environment are due to the fact that their size is comparable with the dimensions of objects such as viruses (about 10−100 nm) or cells (about 1−10 μm). This gives nanoparticles an ability to attach to biological entities without changing their functions, while the high surface-area-to-volume ratio of

Materials for Biomedical Engineering: Inorganic Micro and Nanostructures.
DOI: https://doi.org/10.1016/B978-0-08-102814-8.00008-1

nanoparticles permits strong bonds with surfactant molecules. In environmental applications, the specific features (small size, large surface area) of nanoparticles can provide a tool for very sensitive detection of a specific contaminant from the presence of which pollution often arises. The engineering of nanoparticles can also offer opportunities to treat environmental contamination.

In this chapter we focus on the synthesis, functionalization, and applications of metallic, semiconductor, magnetic, and multifunctional nanoparticles. Compiling all the literature would greatly exceed the scope of this work, instead, we present typical and representative examples for discussion on the synthesis, functionalization, and applications of those nanoparticles.

7.2 SYNTHESIS OF NANOPARTICLES

7.2.1 CHEMICAL REDUCTION

Chemical reduction is an effective wet-chemical method for making zero-valent nanoparticles based on chemical-reducing aqueous salts of metals, such as silver nitrate ($AgNO_3$) in the case of synthesis of silver nanoparticles, for instance. To reduce the precursor metal salt, at least one reducing agent is used to produce electrons for metal ions that reduce them to become zero-valent. Commonly used reductants are borohydride, citrate, and ascorbate. Reduced nanoparticles are stabilized by a stabilizing agent. An example of a stabilizing agent is cetyltrimethylammonium bromide [$(C_{16}H_{33})N(CH_3)_3Br$; CTAB], which is widely used in gold nanoparticle synthesis. The stabilizing agents can be reducing agents themselves, such as citrate of sodium in making silver nanoparticles (Shenava Aashritha, 2013). For more details the reader is referred to the review paper by Alaqad and Saleh (2016) and references therein.

7.2.2 COPRECIPITATION

Precipitation is the carrying down by a precipitate of soluble substances under certain conditions (Patnaik, 2004). Generally, when the concentration of substances reaches supersaturation, a nucleation suddenly appears in solution. The nucleation will be grown by the diffusion on to its surface which then becomes nanoparticles. During the growth, the nucleation needs to be slowed down in order to get uniform nanoparticles. Several methods can be listed as precipitation: coprecipitation, microemulsion/inverse microemulsion, polyol, etc. Coprecipitation is a convenient way to synthesize Fe_3O_4 nanoparticles (Lu et al., 2007; Quy et al., 2013; Dung et al., 2016; Khalil, 2015; Mascolo et al., 2013). The mixture of two chloride salts of $FeCl_2$ and $FeCl_3$ with 1:2 molar ratios of Fe^{2+}/Fe^{3+} was vigorously stirred and kept at 70°C before NH_4OH was added resulting in the black color precipitation. The Fe_3O_4 nanoparticles were collected after purifying through magnetic separation with ethanol and distilled water

several times to decontaminate the residual chemicals. By modifying the pH and ion concentration in solution, the size of nanoparticles can be controlled.

7.2.3 SEEDING

The seeding method was discovered by Frens (1972, 1973), where nanoparticles are grown by the reduction of salt in aqueous solution which contains seed nanoparticles. In this method, the stabilizers are used to control the size and shape of growing nanoparticles. This method was developed over the years using various types of seeding, reductant agents, and stabilizers (Xu et al., 2007; Han et al., 2009; Perrault and Chan, 2009; Ziegler and Eychmuller, 2011; Rioux and Meunier, 2015). For example, the method which was developed by Perrault and Chan in 2009, reduces $HAuCl_4$ in gold nanoparticles seed-contained aqueous solution using hydroquinone. The gold nanoparticle seed can act in conjunction with hydroquinone to catalyze the reduction of gold ions into their surface. If the stabilizer is citrate, typically the seed nanoparticles were prepared by the citrate method. Using this method, the size of nanoparticles can be grown at least 30−300 nm.

7.2.4 MICROEMULSION AND INVERSE MICROEMULSION

Microemulsion is a popular method to synthesize nanoparticles, where microemulsions are an isotropic and thermodynamically stable mixture of "oil," water, and surfactant, or in combination with a cosurfactant. The basic types of microemulsions are direct (oil dispersed in water) and reverse (water dispersed in oil). The small drops of aqueous phase (micelles) may contain salts and/or other ingredients, and the "oil" may actually be the mixture of the surfactants. The reaction to form nanoparticles also can be realized when the micelles mix with each other and the growth of the nanoparticles is controlled by the surfactants in "oil" (Lopez-Quintela and Rivas, 1993). Using this method, the Fe_3O_4 nanoparticles can be synthesized (Feltin and Pileni, 1997) and also can be functionalized with a silica layer. This method can also be used to prepare Fe_3O_4/Au core−shell nanoparticles to prevent the oxidation of magnetic nanoparticles (MNPs) as well as form the biocompatibility (Boutonnet et al., 1982). Furthermore, the inverse microemulsion method is the simplest way to produce multifunctional nanoparticles by creating the silica matrix in aqueous phase, which will fix the single particles inside (Dung et al., 2016).

7.2.5 HYDROTHERMAL METHOD

In the hydrothermal method, the crystals of nanoparticles are grown by heterogenous reaction under conditions of high temperature and high pressure from substances which are insoluble at normal temperature and pressure (Byrappa and Adschiri, 2007). The crystal growth is carried out in an apparatus consisting of a

steel pressure vessel called an autoclave, in which nutrients are supplied along with water. Hydrothermal synthesis is usually carried out below 300°C. The critical condition gives a favorable reaction field for formation of nanoparticles, owing to the enhancement of the reaction rate and large supersaturation based on the nucleation theory. This method has been used to synthesize metal oxide nanoparticles in supercritical water (Hayashi and Hakuta, 2010), metal nanoparticles (Kim et al., 2014), and semiconductor nanoparticles (Bui et al., 2014; Hoa et al., 2011; Williams et al., 2007).

7.2.6 SONOELECTRODEPOSITION

Sonoelectrodeposition is a useful synthesis method for nanoparticles and has been successfully applied to prepare metallic nanoparticles such as FePt and CoPt (Luong et al., 2011; Nam et al., 2012; and references therein). Sonoelectrodeposition is a technique combining the advantages of electrodeposition and mechanical waves of ultrasound to produce metallic nanoparticles (Zhu et al., 2000). In Section 7.4 we discuss silver nanoparticles. One of main disadvantages of the conventional synthesis methods for silver nanoparticles, including chemical reduction, is the presence of unexpected toxic ions in the final products. The toxic ions in the product are mostly the ions of the silver precursor, such as nitrate and thiolsulfate. A good silver precursor such as silver acetate can be used (Irzh et al., 2007), however, this chemical is expensive and manipulation is difficult under ambient conditions. Tuan et al. (2011) reported a modified sonoelectrodeposition technique to obtain silver nanoparticles in a nontoxic solution. The modification is that a silver plate was used as the cathode instead of silver salts thus allowing the avoidance of unexpected ions from the salts.

7.3 FUNCTIONALIZATION/COATING OF NANOPARTICLES

7.3.1 FUNCTIONALIZATION OF NANOPARTICLES

Functionalization of nanoparticles can be defined as the addition of a chemical functional group on their surface in order to achieve surface modification that enables their self-organization and renders them compatible (Subbiah et al., 2010). The most widely used functional groups are amino, biotin, steptavidin, carboxyl, and thiol groups (Bruce and Sen, 2005). The main purpose of functionalizing nanoparticles is to cover their surface with a molecule that possesses the appropriate functionality needed for the designed application. For many biomedicine applications, nanoparticles need to be functionalized in order to conjugate with biological entities such as DNA, antibodies, and enzymes. For more details on the functionalization of nanoparticles, its methods, and class, as well as its implications in biomedical sciences, the reader may be referred to, for instance, the review by Subbiah et al. (2010).

We focus here on the functionalization of gold nanoparticles and MNPs discussed in Section 7.4. For application in detecting breast cancer cells, gold nanoparticles synthesized by a chemical reduction were functionalized with 4-aminothiolphenol (4-ATP, sometimes called *p*-aminothiolphenol [PATP]). For basal cell carcinoma (BCC) detection, different amounts of 4-ATP solutions were added to gold nanoparticles coated by CTAB. CTAB on the surface of gold nanoparticles was replaced by 4-ATP to form gold nanoparticles functionalized with 4-ATP (Au-4ATP). Fe_3O_4 nanoparticles were functionalized using 3-aminopropyl triethoxysilane (APTS). APTS is a bifunctional molecule, an anchor group by which the molecule can attach to free $-OH$ surface groups. The head group functionality $-NH_2$ is for conjugating with biological objects. The amino-NP is ready to conjugate with the DNA of the herpes virus and with the antiCD4 antibody.

7.3.2 SILICA COATING OF MAGNETIC NANOPARTICLES

Maintaining the stability of MNPs for a long time without agglomeration or precipitation is an important issue (see, for instance, Lu et al., 2007). The protection of MNPs against oxidation by oxygen, or erosion by acid or base, is necessary. The common method is protection by a layer which is impenetrable, so that oxygen, for example, cannot reach the surface of the particles. It is noted that the stabilization and protection of particles are often closely linked with each other. One of the ways to protect MNPs is coating them with silica. A silica shell not only protects the magnetic cores, but can also prevent direct contact of the magnetic core with additional agents linked to the silica surface that can cause unwanted interactions. The coating thickness can be controlled by varying the concentration of ammonium and the ratio of tetraethylorthosilicate (TEOS) to H_2O. The surfaces of silica-coated MNPs are hydrophilic, and are readily modified with other functional groups (Ulman, 1996). Quy et al. (2013) and Hieu et al. (2017) have prepared Fe_3O_4/SiO_2 nanoparticles by coating MNPs with silica using TEOS.

7.3.3 MULTIFUNCTIONAL NANOPARTICLES

Recently, multifunctional nanoparticles have gained wide attention due to their advantages in the goal of applications. Potentially, multifunctional nanoparticles which include individual physicochemical properties of nanoparticles, such as plasmonic metallic nanoparticles, photoluminesable semiconductor nanoparticles or quantum dots, and MNPs, can complement some of the limitations of conventional applications using single nanoparticles, particularly in biomedicine. For example, bifunctional nanoparticles which are composed of MNPs and metallic nanoparticles not only can be used as optical labels in bioimaging, diagnosis and therapy, but also allow some biomolecules to be tagged and separated, together with targeted drug delivery and magnetic resonance imaging under the induction of an external magnetic field (Cai et al., 2014; Sotiriou et al., 2011; Ilovitsh et al., 2015; Giani et al., 2012; Sun et al., 2006). Multinanoparticles can be in

core−shell structures or in the complex structures which are a combination of at least two types of single nanoparticles.

Core−shell structured nanoparticles can be classified into inorganic/inorganic, inorganic/organic, organic/inorganic, organic/organic, core/multishell, and movable core/hollow shell nanoparticles (Chaudhuri and Paria, 2012). The synthesis approaches to nanoparticles can be divided into top-down and bottom-up methods. The top-down approaches often use externally controlled tools to cut, mill, and shape materials into the designed nanoscale structures, for example, lithography methods, laser beams, mechanical techniques. The bottom-up approaches exploit the chemical properties of the molecules to cause them to self-assemble to become nanoparticles, such as chemical synthesis discussed above. The bottom-up methods can produce much smaller nanoparticles and are cost-effective, compared to the top-down methods. Both methods are used in the synthesis of core−shell structured nanoparticles. However, since ultimate control is needed for achieving a uniform coating of the shell, the bottom-up approach has proven more suitable. A combination of the two methods can also be utilized, for example, core particles synthesized by the top-down method but then coated by the bottom-up approach in order to maintain precise shell thickness. In general, various methods were used to prepare core−shell nanoparticles. For example, to produce iron oxide@Ag core−shell nanoparticles, several methods were used including impregnation (Liu et al., 2012), surface functionalization followed by deposition (Liu et al., 2010), solvo-thermal reduction (Liu and Li, 2009), and chemical reduction (Hu et al., 2010; Sun et al., 2012). Reducing agents such as glucose and sodium borohydride are used for the reduction of silver salts, and the surface functionalization of iron oxide nanoparticles by different surface-modifying agents is required. Hu et al. (2010) used glucose for the reduction of $Ag(NH_3)_2^+$ to Ag, which is adsorbed onto the surface of silica-coated iron oxide which is prepared by the coprecipitation method. Liu et al. (2010) have reported the surface functionalization of Fe_3O_4 surface by APTS followed by reduction of $AgNO_3$ using sodium citrate and sodium borohydride. Sun et al. (2012) have used sodium borohydride as the reducing agent for the reduction of $Ag(NH_3)_2^+$ to obtain Fe_3O_4@Ag core−shell nanoparticles. Dung et al. (2016) used ultrasound to assist in the reduction of silver ions following this strategy. Liu and Li (2009) have used dimethylformamide as the reducing agent during solvo-thermal synthesis of γ-Fe_2O_3@Ag microspheres. In parallel, one-step synthesis using thermal decomposition of silver acetate in the presence of iron oxide microspheres is also applicable and does not require the addition of any external reducing agent or surface modification of iron oxide (Sharma and Jeevanandam, 2013). To control the overall size and the shell thickness, a microemulsion method, where water droplets act as a template or nanoreactor, is preferable to a bulk medium.

Other types of multifunctional nanoparticles are the complex structures of materials, which is the combination of at least two types of single nanoparticles. Similar to a core−shell structure, the nanomaterials used in complex structures

can be categorized by two types of nanoparticles: organic, which includes micelles, liposomes, nanogels, dendrimes, and inorganic, which includes magnetic, semiconductor, lanthanide, and metallic nanoparticles. The combination can be achieved in many ways, however it is needed to fulfill the requirements of the applications. For example, the multifunctional nanoparticles should have superparamagnetic properties in order to be applied in drug delivery and DNA separation, and they should have plasmonic properties in order to be applied as biolabeling agents, and they should also be biocompatible. The simplest combination which fulfills these requirements is the complex of Fe_3O_4 nanoparticles with superparamagnetic properties and Ag nanoparticles with plasmonic properties in a matrix of SiO_2 which provide the biocompatibility and also improve the stability of Ag and Fe_3O_4 nanoparticles. Surface activator polyvinylpyrrolidone (PVP) was used to control the size of silver nanoparticles, which were synthesized by a wet-chemical reduction method with $NaBH_4$ as reductant. The synthesized nanoparticles were coated with 4-ATP to form functionalized Ag-4ATP nanoparticles. These functionalized nanoparticles were combined with the above-prepared Fe_3O_4 nanoparticles by an inverse microemulsion method to form multifunctional nanoparticles (Dung et al., 2014). In this method, the microemulsion was created by mixing the hydrophilic phase of the mixture of Ag-4ATP and Fe_3O_4 solution and the hydrophobic phase of toluene. The mixture of Ag-4ATP/Fe_3O_4 with different mass rates was moderated under a sonic bath for 2 hours, then TEOS was added to react with water in solution as in reaction (7.1). The formed SiO_2 coating layer in amorphous conformation covers both initial particles.

$$Si(OC_2H_5)_4 + 2H_2O \rightarrow SiO_2 + 4C_2H_5OH \tag{7.1}$$

The multifunctional composites were also successfully prepared in a complex form using an ultrasound-assisted chemical method (Dung et al., 2017a). MNPs were firstly prepared by the coprecipitation method, then coated by a silica layer. The silica layer, after that, was modified by APTS. Silver ions were then absorbed on the surface of APTS-functionalized silica-coated MNPs. Under the ultrasonic wave of 200 W acting for 60 minutes these silver ions were reduced by sodium borohydride. In XRD characterization after synthesis, the relative intensity of diffraction peaks of silver crystals increases when the atomic ratio of silver to iron increases from 0.208 to 0.455. In parallel, all nanoparticles showed superparamagnetic properties with the saturation magnetization decreased from 44.68 to 34.74 emu/g with increasing silver:ion atomic ratio. The coexistence of strong surface plasmon absorption at 420 nm and these superparamagnetic properties make these particles promising for biomedical applications.

In another way, MNPs can be directly functionalized with an amino group without coating by silica layer (Dung et al., 2017b). In this way, Fe_3O_4-ZnO multifunctional nanoparticles were successfully synthesized in aqueous solution by ultrasound-assisted thermolysis. The as-prepared Fe_3O_4 MNPs were modified by APTS to have free amine ($-NH_2$) groups on their surface. Zn^{2+} ions then were

added and stirred to adsorb onto the surface of Fe_3O_4-NH_2 nanoparticles in alkaline solution at pH 11. The solution was decomposed through thermolysis in an ultrasound bath. The characterization shows that photoluminescence of Fe_3O_4-ZnO multifunctional nanoparticles was enhanced in visible light at a wavelength of 565 nm to allow detection, labeling, diagnosis, and therapy in biomedicine. Furthermore, they exhibit superparamagnetic properties of Fe_3O_4 with high saturation magnetization, which can be used for separation applications in biomedicine under an external magnetic field.

7.4 APPLICATIONS

7.4.1 APPLICATION OF GOLD NANOPARTICLES FOR BREAST CANCER CELL DETECTION

Gold nanoparticles are promising candidates for cell imaging and tumor-targeted drug delivery (Sokolov et al., 2003; Paciotti et al., 2004; Jain, 2005), breast cancer diagnosis, and targeted therapy (Yezhelyev et al., 2006). Being a member of the epidermal growth factor receptor tyrosine kinase family, HER2 is found to be overexpressed in 20%−30% of human breast cancers (Harries and Smith, 2002; and references therein). Therefore, HER2 is an interesting target for breast cancer therapies. Anti-HER2 (trastuzumab, trade name Herceptin) is a humanized monoclonal antibody (mAb) designed specifically for antagonizing the HER2 function. Quynh et al. (2011) and Nguyen et al. (2015) have synthesized gold nanoparticles by a chemical reduction then applied them for imaging KPL4 breast cancer cells after conjugating them with trastuzumab.

Fig. 7.1 shows the bright-field and dark-field microscopy images of breast cancer cells after being incubated with gold nanoparticles nonconjugated with trastuzumab as well as conjugated with trastuzumab (Nguyen et al., 2015). As can be seen from Fig. 7.1, when the gold nanoparticles were not conjugated with trastuzumab, the dark-field image showed no signal of the gold nanoparticles (A_2). When the gold nanoparticles were directly conjugated with trastuzumab, the gold nanoparticles were bound onto cancer cells and these cancer cells were clearly observed in the dark-field image (A_4) through the scattering light from the gold nanoparticles. When the 4-ATP functionalized gold nanoparticles (amino-gold nanoparticles) were covalently conjugated with trastuzumab through l-ethyl-3-(3-dimethylaminopropyl) ethylcarbodiimide (EDC) connection, the gold nanoparticles also concentrated on the cancer cells, but these cancer cells were observed with slightly lower intensity in the dark-field image (A_6) compared to those in image A_4. Nguyen et al. (2015) pointed out, however, that the gold nanoparticles directly conjugated with trastuzumab could be stored in a freezer for only about 2 weeks before they lost their activity, while the gold nanoparticles covalently conjugated with trastuzumab were stable with storage for about two months.

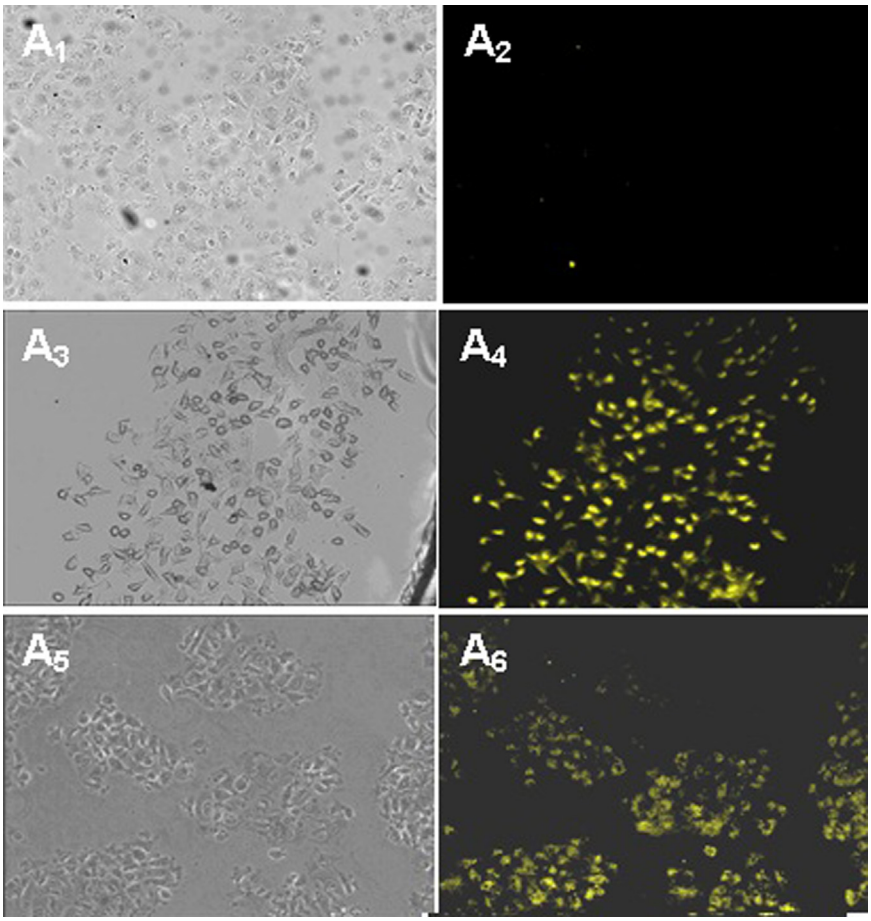

FIGURE 7.1

Bright-field (A_1, A_3, A_5) and dark-field (A_2, A_4, A_6) microscopy images of breast cancer cells after being incubated with gold nanoparticles nonconjugated with trastuzumab (A_1, A_2), the gold nanoparticles conjugated with trastuzumab (A_3, A_4) and the amino-gold nanoparticles covalently conjugated with trastuzumab through EDC connection (A_5, A_6).

After Nguyen, H.L., Nguyen, H.N., Nguyen, H.H., Luu, M.Q., Nguyen, M.H., 2015. Nanoparticles: synthesis and applications in life science and environmental technology. Adv. Nat. Sci.: Nanosci. Nanotechnol. 6, 015008.

7.4.2 BASAL CELL CARCINOMA FINGERPRINTED DETECTION

Skin cancer is the most common cancer in humans and its incidence is increasing (Baxter et al., 2012). Worldwide, BCCs constitute about 74% of skin cancer cases (NCIN, 2013). Among the treatments for "high-risk" BCCs (i.e., BCCs on the

face and neck, or recurrent BCCs), Mohs micrographic surgery (MMS) is the most efficient (Mohan and Chang, 2014). This procedure helps to maximize the removal of tumor cells, while spares as much healthy tissue as possible. However, the need for a pathologist or specialized surgeons to diagnose frozen sections during surgery has limited the wider use of MMS, which leads to cases of inappropriate inferior treatment. Frozen-section histopathology also requires arduous and time-consuming procedures, increasing the costs compared to standard methods of BCC excision.

For skin cancer diagnosis, Raman spectroscopic imaging is a promising technique, because of its high sensitivity to molecular and structural changes associated with cancer. However, raster scanning Raman mapping requires long times for data acquisition, typically days for tissue specimens of 1 cm $\times$ 1 cm. Recently, multimodal spectral imaging based on Raman spectroscopy and tissue autofluorescence was used to reduce the BCC diagnosis time to only 30−60 minutes, which becomes suitable for use during MMS (Kong et al., 2013; Takamori et al., 2015).

An alternative method that could allow to reduce data acquisition and BCC diagnosis times during MMS is surface-enhanced Raman spectroscopy (SERS). It was discovered that strongly increased Raman scattering signals can be obtained in the very close vicinity of metal nanostructures, which are mainly due to resonances between optical fields and the collective oscillations of the free electrons in a metal. Thus SERS has attracted great interest in the biolabeling field because significant enhancement of the labeling signals of molecular vibrations on the metallic nanoparticles surface can be obtained. Quynh et al. (2016) studied surface-enhanced Raman (SER) signal of 4-ATP that was linked to the surface of gold nanoparticles conjugated with skin carcinoma cell antibody BerEP4. Gold nanoparticles with sizes ranged from 2 to 5 nm were prepared by a wet-chemical method using CTAB. The Au-4ATP-antibody solutions were dropped on the surface of the tissue sample and the SER scattering signals were collected and analyzed. Fig. 7.2 shows the fingerprinted landscape of SER signals of Au-4ATP-antibody on a BCC tissue. Fig. 7.2A shows the colored image of a Gram-stained tissue, where the cancer cell area may be the dark-colored regions, for example, region A1, A2. However, the result of diagnosis essentially depends on the subjective decision of the pathologists because this nonspecific method may lead to misinterpretation of noncancer regions as cancer ones. Fig. 7.2B shows a bright-field microscopy image of the tissue, where B1 region corresponds to a hair follicle position, and B2 does not, although B1 and B2 have the same position on the tissue as regions A1 and A2 in Fig. 7.2A. Fig. 7.2C shows the result of an SER signal obtained by the principal component analysis (Quynh et al., 2016). Fig. 7.2D shows the result of the SER signal analyzed using only the intensity of SER peaks at 1075 cm^{-1}. The Au-antibody colloids are oriented close to the BCC surface by the antigen−antibody coupling. The carcinoma sections act as a dock where a high concentration of Au-4ATP-antibody particles is distributed, then the SER peak intensity at 1075 cm^{-1} will be higher in these areas. In

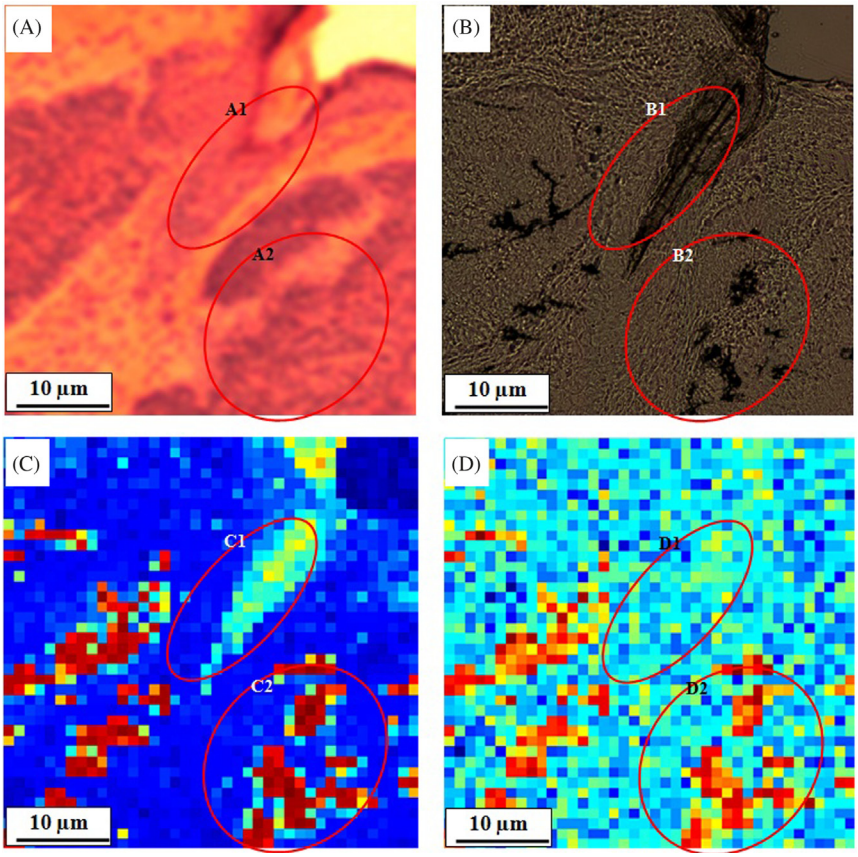

FIGURE 7.2

Fingerprinted landscape of SER signals of Au-4ATP-antibody on BCC tissue. (A) Image of Gram-stained BCC tissue where A1 and A2 are the areas of suspected BCC; (B) bright-field microscopy image of tissue, where regions B1 and B2 are in the same position on the tissue as regions A1 and A2, respectively; (C) SER signal landscape obtained by principal component analysis, where regions C1 and C2 are in the same position on the tissue as regions A1 and A2, respectively; (D) the fingerprinted landscape of intensity of SER peaks at 1075 cm^{-1}, where regions D1 and D2 are in the same position on the tissue as regions A1 and A2, respectively. The difference between D1 and D2 shows that only red-colored D2 (and the similar-colored area) are the infected area, while D1 is not.

After Quynh, L.M., Nam, N.H., Kong, K., Nhung, N.T., Notinger, I., Henini, M., et al., 2016. Surface-enhanced Raman spectroscopy study of 4-ATP on gold nanoparticles for basal cell carcinoma fingerprint detection. J. Electron. Mater. 45, 2563–2568.

Fig. 7.2C, the colored areas such as C1 and C2 can be considered as cancer regions. However, in Fig. 7.2D the area D1 does not show the high intensity of the peak at 1075 cm^{-1}, while the others, such as the D2 area, indicate very high intensity of the peak at 1075 cm^{-1}. From Fig. 7.2, only A2, B2, C2, and D2 regions can be definitely considered as the cancer areas, while A1, B1, C1, and D1 may assigned as the position of hair follicles where the cell concentration is higher than in other parts. Quynh et al. (2016) pointed out that, while the whole SER map collecting time should be longer than 2 hours (the collecting time of each spectrum was nearly 5 seconds), the fingerprinted image using peak height at 1075 cm^{-1} can be observed in around 5 minutes. Hence, this method may represent a solution for quick diagnosis, even during operation.

7.4.3 ANTIBACTERIAL TEST USING SILVER NANOPARTICLES

Silver nanoparticles (AgNPs) are commonly utilized nanomaterials due to their antibacterial properties, high electrical conductivity, and unique optical properties that can be used in various applications (Sondi and Salopek-Sondi, 2004). It is believed that the high affinity of Ag toward sulfur or phosphorus is the key element of its antibacterial property. As sulfur and phosphorus are found in abundance throughout cell membranes, AgNPs react with sulfur-containing proteins inside or outside the cell membrane, which in turn affects cell viability (Pal et al., 2007; Elechiguerra et al., 2005). Another theory proposed that Ag^{+} ions released from AgNPs can interact with phosphorus moieties in DNA, resulting in inactivation of DNA replication, or can react with sulfur-containing proteins to inhibit enzyme functions (Sharma et al., 2009). These properties allow the incorporation of AgNP into various matrices such as activated carbon (AC), polymer networks, textiles, and wound dressing materials (Sedaghat and Nasseri, 2011).

Many approaches have been developed to obtain AgNP of various shapes and sizes, including chemical reduction, laser ablation, gamma irradiation, electron irradiation, chemical reduction by inorganic and organic reducing agents, photochemical method, microwave processing, thermal decomposition of Ag oxalate in water and in ethylene glycol, and sonoelectrochemical method (see references in Tuan et al., 2011). As pointed out in Section 7.2.6, one of main disadvantages of those methods is the presence of unexpected toxic ions in the final products. Tuan et al. (2011) report a modified sonoelectrochemical technique to obtain AgNP in a nontoxic solution. The silver particles are then directly loaded on AC produced by thermal activation of coconut husk. Here we concentrate to their work on the antibacterial properties of AgAC examined by inhibition growth of *Escherichia coli*. Fig. 7.3 shows the quantitatively antibacterial study of AgNP in Luria-Bertani (LB) broth. It presents the dynamics of *E. coli* growth in only LB broth (negative control), TSC control [LB broth supplemented with 120 μL trisodium citrate (TSC) solution], and AgNP antibacterial tests (LB broth supplemented with AgNP of concentration from 2 to 200 μg/mL). In this figure, OD_{595} represents optical density at 595 nm (1 optical density at 595 nm, OD_{595}, equals the

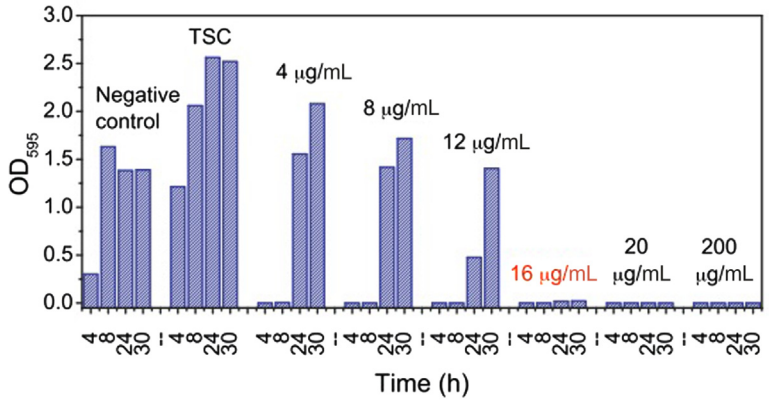

FIGURE 7.3

Bar chart of optical density at 595 nm, OD_{595}, presenting *Escherichia coli* concentration in LB in the presence of different concentrations of AgNP (μg/mL) as a function of time (h). Each test was conducted after 4, 8, 24, and 30 h. It is clear that, with the concentration of AgNP $\geq$ 16 μg/mL, *E. coli* growth was inhibited.

After Tuan, T.Q., Son, N.V., Dung, H.T.K., Luong, N.H., Thuy, B.T., Anh, N.T.V., et al., 2011. Preparation and properties of silver nanoparticles loaded in activated carbon for biological and environmental applications. J. Hazard. Mater. 192, 1321–1329.

concentration of 1.7×10^9 cells/mL). The initial number of *E. coli* inoculated into 2 mL LB medium of the tested tube was 1.7×10^6 cells, giving the final bacterial concentration of 8.5×10^5 cells/mL. It is observed that *E. coli* grew normally in the negative control and the TSC control. After 30 hours in the TSC control, the concentration of *E. coli* ($OD_{595} = 2.5$) is higher than that in the negative control ($OD_{595} = 1.5$) which suggests that TSC was not toxic to *E. coli* and may be even enabled for the growth of the bacteria. With the presence of AgNP, the situation is different because of the well-known antibacterial property of AgNP (Kim et al., 2007). When AgNP concentration was 2 μg/mL, the result is similar to that of the negative control because the low value of AgNP could not inhibit bacterial growth. With a higher AgNP concentration, the inhibitory effect appeared within 8 hours even at a low AgNP concentration of 4 μg/mL. Fig. 7.3 clearly shows that, with the concentration of AgNP > 16 μg/mL, the *E. coli* growth was inhibited.

7.4.4 MAGNETIC NANOPARTICLES

MNPs are of great interest in biomedicine applications. In the applications described below these nanoparticles were synthesized by the coprecipitation method.

7.4.4.1 Arsenic removal from water

MNPs Fe_3O_4 were reported to adsorb arsenic ions from contaminated water (Leslie-Pelecky et al., 2005). In this environmental application, compared to other techniques currently used to remove arsenic from contaminated water, such as centrifuges and filtration systems, this method using MNPs has the advantage of being simple, and, most importantly, not requiring electricity. This is very important, because arsenic-contaminated sites are often found in remote areas with limited access to power (Filipponi and Sutherland, 2010).

The arsenic adsorption abilities of Fe_3O_4, $Fe_{1-x}Co_x{\cdot}Fe_2O_3$ (Co-ferrites) and $Fe_{1-y}Ni_yO{\cdot}Fe_2O_3$ (Ni-ferrites) with $x = 0$, 0.05, 0.1, 0.2, 0.5 and $y = 0.2$, 0.4 were studied with different conditions of stirring time, concentration of nanoparticles, and pH (Hai et al., 2008). The starting arsenic concentration of 0.1 mg/L was reduced about 10 times down to the maximum permissible concentration (MPC) of 0.01 mg/L after a few minutes of stirring. The removal process seemed not to depend considerably on the concentration of x in the Co-ferrites. Similar results were found for the Ni-ferrites, where the arsenic concentration was reduced to the MPC value after a stirring time of a few minutes and the removal did not change considerably with y. Studying also the effects of the weight of the nanoparticles on the removal process, Hai et al. (2008) showed that, after 3 minutes of stirring, the optimal weight to reduce arsenic concentration down to a value lower than the MPC was 0.25 g/L for Fe_3O_4 and 0.5 g/L for Co- and Ni-ferrites. Studying the desorption process, Hai et al. (2008) showed that 90% of the arsenic ions was desorbed from nanoparticles. After desorption, the nanoparticles did not show any difference in arsenic readsorption ability. Repeating the adsorption−desorption process four times, Hai et al. (2008) proved that the nanoparticles could be reused for arsenic removal.

7.4.4.2 Herpes DNA separation

Herpes simplex virus, or herpes, causes extremely painful infections in humans (Ryan and Ray, 2004). Thus, the determination of the presence of herpes is important. A simple and fast way to recognize the presence of the DNA of the virus is to use an electrochemical sensor. However, electrochemical sensors exhibit a sensitivity limit, so they cannot measure concentrations lower than a few tens of nM/L (Tuan et al., 2005). Therefore, a virus DNA separation before the measurement by using the electrochemical sensor is needed in order to increase the concentration of the DNA. Hai et al. (2008) used a DNA sequence, which is representative of the herpes, as a probe to hybridize with the target DNA in the sample. After being activated with EDC and 1-methylimidazole (MIA), the probe DNA was mixed with the amino-NP to have nanoparticles with the probe DNA on the surface (DNA-NP). The herpes DNA separation was carried out as follows: 1 mL of the solution containing 2 wt.% of DNA-NP was mixed with 2−20 mL of a solution with 0.1 nM/L of the herpes DNA. The hybridization of the probe DNA and the target DNA appeared at 37°C for 1 hour. Then, the

nanoparticles with hybridized DNA were collected and redispersed in 0.1 mL of water using magnetic decantation. The dehybridization of the nanoparticles with the probe and target DNA was obtained at 98°C. Hai et al. (2008) obtained a solution with a high concentration of the DNA of the herpes virus after removing the DNA-NP from the solution by using magnetic decantation. When all the target DNA were separated, the DNA concentration had increased from 20 to 200 times. Fig. 7.4 shows the dependence of the output signal on the initial volume of the solution containing 0.1 nM/L of the herpes DNA before and after the magnetic separation (Hai et al., 2008). The initial solution contained 0.1 nM/L of the DNA, which was much smaller than the sensor sensitivity. Therefore, the output signals before magnetic enrichment were almost zero (Fig. 7.4, *open squares*). After magnetic enrichment, the output signals linearly increased with increasing initial solution volume, depending on the initial volume of the solution. The higher the volume, the higher the concentration. The result is higher output signals were obtained. This means that the concentration of the herpes DNA was much higher after the enrichment. With the highest initial volume that Hai et al. (2008) used in their studies, the concentration after magnetic enrichment was 200 times higher than the initial concentration.

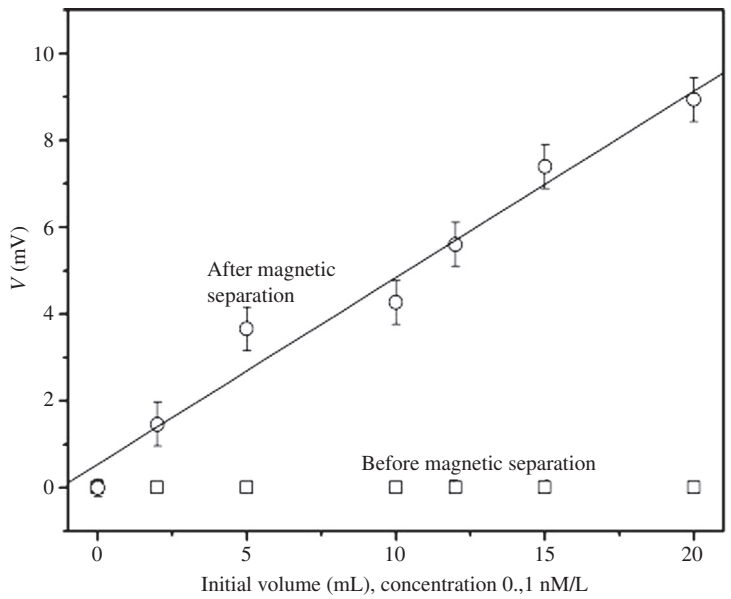

FIGURE 7.4

Dependence of the output signal on the initial volume of solution containing herpes DNA before and after magnetic separation.

After Hai, N.H., Chau, N., Luong, N.H., Anh, N.T.V., Nghia, P.T., 2008. Application of magnetite nanoparticles for water treatment and for DNA and cell separation. J. Korean Phys. Soc. 53, 1601–1606.

7.4.4.3 $CD4^+$ cell separation

In human immunodeficiency disease, such as HIV/AIDS, helper T cells ($CD4^+$ T cells) are considerably destroyed by HIV. For mechanisms of $CD4^+$ T cell depletion in HIV infection we refer the reader to the review of, for instance, Okoye and Picker (2013). A dropping number of $CD4^+$ T cells (which are often referred to as CD4 cells) in blood is an indicator of immunodeficiency as in the case of HIV/AIDS. The number of $CD4^+$ T cells in the blood of HIV-infected patients is often reduced to less than 500 cells/μL. According to the World Health Organization (WHO) classification, a person is diagnosed with AIDS if the CD4 count is less than 200 cells/μL (World Health Organization, 2007). Thus, the CD4 count is very important for doctors to adjust treatment strategies. The principle of counting the number of $CD4^+$ T cells in blood is based on the specific linker between the antiCD4 monoclonal antibody and $CD4^+$ T receptor on the lympho T surface (Casset et al., 2003; and references therein). Fluorescent-labeled antiCD4 antibody has been commonly used to count $CD4^+$ T cells of HIV/AIDS patients due to its binding specificity to the cells and fluorescent emission signals. However, the fluorescent signals of labeled $CD4^+$ T cells are sometimes interfered with by autofluorescence of other dead white cells, such as killers ($CD8^+$) T cells, B cells, macrophages, or neutrophils, which contribute to the background in detection. To minimize this background interference, $CD4^+$ T cells can be magnetically sorted from other cells in the blood, followed by fluorescent signal detection.

Hai et al. (2008) and Khuat et al. (2008) used Fe_3O_4 MNPs coated with fluorescent-labeled antiCD4 antibody (antiCD4-MNPs) to count the $CD4^+$ T cells. The antiCD4-MNPs were prepared through covalent linking between the carboxyl group of the antiCD4 antibody and the amino group of amino-modified MNPs. The antiCD4-MNPs were then used as a material to conjugate with $CD4^+$ T cells for magnetic separation. These authors observed a number of cells bound with magnetic clusters and particles. Fig. 7.5 shows the conventional microscope visualization of the blood cells after being coupled with the antiCD4 antibody and antiCD4-MNPs and separated using a magnet (Hai et al., 2008). For observing the $CD4^+$ T cells, using fluorescence isothiocyanate labeled antiCD4-MNPs, the fluorescent intensity was improved by about two times compared to when cells were only labeled with the antiCD4 antibody. This result indicates the role of the MNPs and can be used for the treatment of an HIV-infected patient with a simple fluorescent microscope.

7.4.4.4 Detection of pathogenic viruses

Purification of nucleic acids (DNA and RNA) from clinical samples is an important step in diagnostics, such as detection of pathogenic viruses and bacteria using the polymerase chain reaction (PCR), paternity testing, genetic research, DNA fingerprinting, and DNA sequencing. The nucleic acid purification method based on interaction with silica, developed by Boom et al. (1990), is commonly used. It

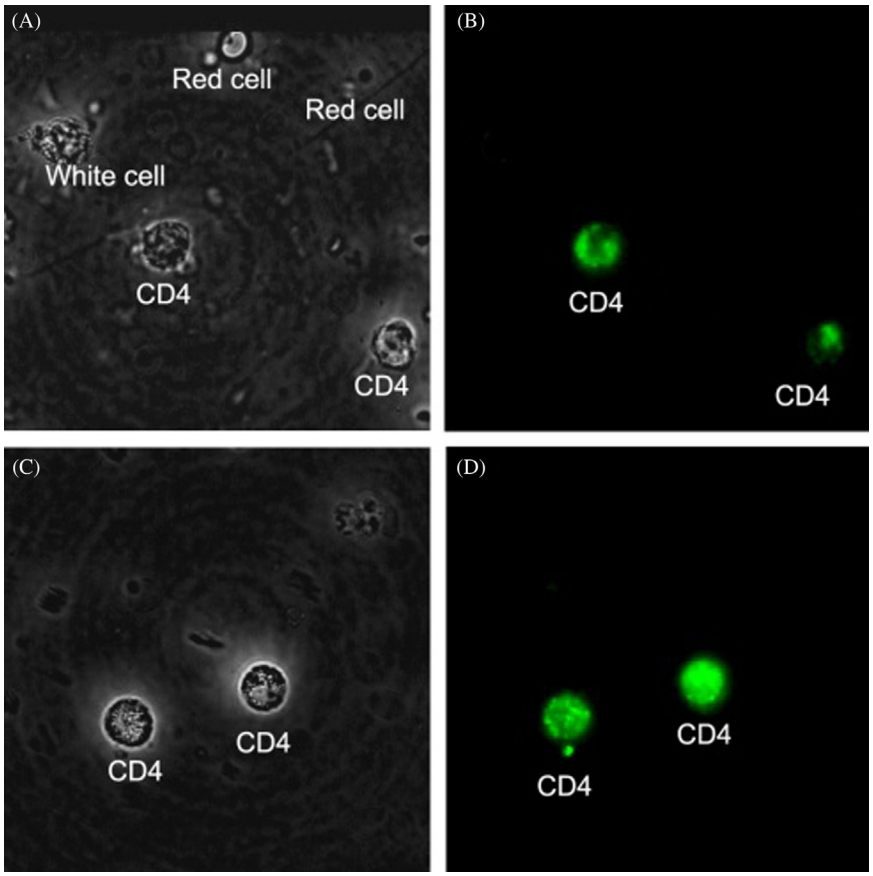

FIGURE 7.5

Microscope visualization of the blood cells under white light (A, C) and under blue light excitation (B, D), after being coupled with the antiCD4 antibody and antiCD4-MNPs and separated by using a magnet.

After Hai, N.H., Chau, N., Luong, N.H., Anh, N.T.V., Nghia, P.T., 2008. Application of magnetite nanoparticles for water treatment and for DNA and cell separation. J. Korean Phys. Soc. 53, 1601–1606.

is known that DNA binds to silica, even though both DNA and the silica surface are negatively charged. Thus, to provide insight into important issues such as the mechanism behind DNA binding to silica is of great interest. Using molecular dynamics simulations, Shi et al. (2015) showed that the two major mechanisms for binding of DNA to silica are attractive interactions between DNA phosphate and surface silanol groups and hydrophobic bonding between DNA base and hydrophobic region of silica surface. These short-range attractions can be sufficiently strong to overcome the electrostatic repulsion between negatively charged DNA and negatively charged silica surface.

Micrometer-size silica-coated magnetic beads have been developed by different groups (see, for instance, Akutsu et al., 2004) and biotech companies such as Roche Diagnostics, Life Technologies, Promega, and Beckman Coulter to improve the efficiency of purification. Berensmeier (2006) described methods based on magnetic microparticles for nucleic acid purification. Recently, the investigation and application of silica-coated MNPs for separation and purification of nucleic acids has become an emerging area. Ashtari et al. (2005) reported a method for recovery of target ssDNA using amino-modified silica-coated MNPs and used them to recover trace concentrations of target ssDNA fragments of severe acute respiratory syndrome virus with high efficiency and good selectivity. Quy et al. (2013) presented a method for synthesis of the silica-coated Fe_3O_4 MNPs and their application for isolation and enrichment of DNA of Epstein−Barr virus (EBV), which is associated with particular cancers and lymphoma, and hepatitis virus type B (HBV) which causes hepatitis. Quy et al. (2013) have shown that the purification efficiency of DNA of both EBV and HBV using synthesized silica-coated Fe_3O_4 MNPs was superior to that obtained with commercialized silica-coated Fe_3O_4 magnetic microparticles. Quy et al. (2013) reported also on time saving in detection of EBV and HBV, namely the time required for DNA purification using silica-coated Fe_3O_4 nanoparticles was significantly reduced as the particles were attracted to magnets more quickly (15−20 seconds) than the commercialized silica-coated Fe_3O_4 microparticles (about 2−3 minutes). These results were attributed to the fact that silica-coated Fe_3O_4 nanoparticles have a larger total surface area compared to that of the commercialized silica-coated Fe_3O_4 microparticles.

7.4.4.5 Specific and rapid tuberculosis detection

The worldwide effort to eradicate tuberculosis (TB), the highly infectious disease caused by *Mycobacterium tuberculosis* (MTB), has thus far led to significant decreases in the number of incidents and mortality rates. TB, however, remains the second leading cause of death from an infectious disease and a major global health problem (World Health Organization, 2011). Unfortunately, in the absence of an effective screening method, there are many cases of TB and multidrug-resistant-TB which are not opportunely detected or treated. In the early 1990s, a diagnostic procedure based on the amplification of the insert sequence (IS) 6110 was developed and soon became prevalent. This method is displaying advantages regarding detection limit and specificity through the amplification of this signature sequence using the PCR technique (Kolk et al., 1992, 1998; Kox et al., 1994; Sankar et al., 2011; Shukla et al., 2011). However, this procedure requires the time-consuming extraction of DNA from each sample, including a cell lysis step which is usually inefficient on account of the highly complex bacterial cell wall (Noordhoek et al., 1994; Ellis and Zabrowarny, 1993; Ogbaini-Emovon, 2009).

Recently, the collaboration between biologists and physicists has allowed the development of nanomaterials in DNA extraction from different organisms. More importantly, using MNPs, multiple samples could be processed simultaneously on

a microtiter plate, which would enhance the testing rate and reduce the contamination risk for testing personnel, especially in the case of dangerous pathogens (e.g., TB). Furthermore, this material could be constructed to form bioconjugates containing specific antibodies which would enhance the specificity of the detection method (Arruebo et al., 2009). Recently, Pham et al. (2015) reported for the first time the development of a specific and rapid TB detection using MNPs. The MNPs were functionalized with amino groups to facilitate coupling with anti-TB antibodies. The coupled nanoparticles were used to enrich *Mycobacterium.* In addition, preliminary assessment of this method in testing clinical samples (sputum and throat wash specimens) was also noted. The results of this study indicated potential for the establishment of a high-throughput semiautomated TB diagnostic procedure, which is currently being studied. Specificity, or the capability of improving signal-to-noise ratio, is a critical criterion in any diagnostic procedure. Samples collected from patients (sputum in most cases) normally contain other microorganisms which might be the contamination source. By pretreatment with *N*-acetyl L-cysteine-sodium hydroxide (NALC-NaOH), the decontamination could be done for sputum samples. This technique, however, could not eliminate nonspecific signal entirely. Besides the specifically designed primers for the amplification of the signature sequence IS6110, the coupled anti-MTB antibody served as a sieve which captured only the MTB antigens. The whole procedure was done in approximately one hour, which was half of the total time required for the traditional DNA extraction method.

7.4.4.6 *Biological treatment targeting* Mycobacterium tuberculosis *in contaminated wastewater*

Wastewater from hospitals and facilities receiving patients infected with contagious microorganisms has dense concentrations of these pathogens, which may represent a danger to public health. Therefore, proper wastewater treatment to remove these contaminants before discharging to the sewage system is a great societal concern. Most common wastewater treatment methods are divided into physical (heating, ultraviolet radiation, etc.), chemical (e.g., hypochlorite/chlorination, ozonation), and biological categories. The main disadvantages of the first two categories are complex implementation and high maintenance cost (e.g., due to corrosion of the pipe systems). With the additional advantage of being environmentally friendly, biological methods have become valuable alternatives. Most of these methods utilize live microorganisms in either fermentation processes to remove toxic chemicals or filtration applications through the formation of biofilm (Sewage water treatment vat., 2016) and, thus, are without specific targets. Nguyen et al. (2016) reported biological treatment targeting MTB in contaminated wastewater using lysing enzymes coupled to Fe_3O_4 MNPs. This study was a further development from previous results obtained with a complex comprised of magnetic amino nanoparticles and anti-TB antibody molecules (Pham et al., 2015). The complex, referred to as NP-NH_2-anti-TB, was shown to be capable of specifically capturing MTB (Pham et al., 2015), which would be killed with the

addition of lysing enzymes. The major role of the nanoparticles is to bring these molecules in close proximity so that the lysing enzymes can work on the bacteria captured through the conjugated antibody on the same surface area. This, ideally, would solve the limit of diffusion, thus enhancing the reaction rate. Nguyen et al. (2016) also reported an initial assessment of the developed method in a wastewater model by spiking the wastewater samples collected from a hospital and a facility receiving TB patients with *Mycobacterium bovis* from bacillus Calmette-Guérin vaccine. The results of this study indicated potential applications of the NP-NH_2-anti-TB complex combined with enzymes to efficiently treat MTB-contaminated wastewater.

7.4.5 APPLICATIONS OF MULTIFUNCTIONAL NANOPARTICLES

Multifunctional nanoparticles are gradually attracting more and more attention because of their ability to combine numerous properties, such as electronic, magnetic, optical, and catalytic. They are highly functional materials with modified properties which can be quite different from those of the individual materials. The properties of core−shell nanoparticles can be modified by changing either the constituting materials or the core-to-shell ratio (Oldenburg et al., 1998). Multifunctional nanoparticles show distinctive properties of the different materials employed together to meet the diverse application requirements. The purpose of the functionalization is manyfold, such as surface modification, the ability to increase the functionality, dispersibility, and stability, controlled release of the single nanoparticles, reduction in consumption of materials, etc. Applications of different multifunctional nanoparticles are summarized in review articles by Karele et al. (2006), Seleci et al. (2016), Jia et al. (2013), and Bao et al. (2013). The multifunctional nanoparticles are widely used in various applications such as pharmaceutical applications (Caruso, 2001), biomedical (Balakrishnan et al., 2009; Salgueirino-Maceira and Correa-Duarte, 2007), catalysis (Daniel and Astruc, 2004; Phadtare et al., 2003), electronics (Kortan et al., 1990; Qi et al., 1996), enhancing photoluminescence (Mews et al., 1994; Kamat and Shanghavi, 1997), creating photonic crystals (Scodeller et al., 2008), etc. Especially in the biomedical field, these nanoparticles are used for bioimaging (Laurent et al., 2008; Babes et al., 1999; Dresco et al., 1999), controlled drug release (Dresco et al., 1999), targeted drug delivery (Laurent et al., 2008; Gupta and Gupta, 2005; Dresco et al., 1999; Yan et al., 2009), cell labeling (Laurent et al., 2008; Jaiswal et al., 2003; Michalet et al., 2005), and tissue engineering applications (De et al., 2008). For instance, core−shell nanoparticles have attracted considerable attention in clinical and therapeutic applications (Hirsch et al., 2003; Loo et al., 2004). Core−shell nanoparticles, which are strong absorbers, can be used in photothermal therapy, while those which are efficient scatterers can be used in imaging applications. Silica core−gold shell nanoshells, a novel core−shell nanostructure, which either absorb or scatter light effectively, can be designed by varying their core-to-shell ratio (Loo et al., 2004). In imaging applications of core−shell

nanoparticles, they can be conjugated with specific antibodies for diseased tissues or tumors. When conjugated nanoparticles are inserted in the body, they get attached to diseased cells and can be imaged. In parallel, when the tumor has been located, resonance wavelength absorption of the core−shell nanoparticles will lead to localized heating of the tumor and it is destroyed. In other words, the imaging and photothermal therapy can be carried out together with core−shell or multifunctional nanoparticles. In drug-delivery systems using core−shell nanoparticles, the drug can be encapsulated or adsorbed onto the nanoparticle surface (Sparnacci et al., 2002) via a specific functional group or by an electrostatic stabilization technique. The nanoparticles will come into contact with the biological medium, and then direct the drug. For instance, the enzyme- and antibody-conjugated core−shell nanoparticles, which are strong absorbers with gold shells, can be embedded in a matrix of the polymer, such as nisopropylacrylamide (NIPAAm), and acrylamide (AAm) (West and Halas, 2000). These polymers exhibit a melting temperature which is slightly above body temperature. If the core−shell nanoparticles absorb heat from the illumination with resonant wavelength, the heat will transfer to the local environment, then cause collapse of the polymer matrix and release of the drug. Furthermore, when the core is MNPs, the core−shell nanoparticles with the bifunction of magnetic and gold nanoparticles can drive the drug and kill the tumor under the external magnetic field as well as by the irradiation of resonance wavelength. The usual methods of tumor treatment, such as chemotherapy or radiotherapy, have various side effects such as substantial loss of hair, lack of appetite, diarrhea, etc. The process of attacking the tumor also leads to the loss of many healthy cells. Core−shell or multifunctional nanoparticles offer an effective and relatively safer strategy to cure these ailments by significantly reducing the amount of chemicals or radiation using local treatments.

Another strategy of using multifunctional nanoparticles is using multiple types of nanoparticles in one application, such as in fast DNA diagnosis (Quynh et al., 2014). This fast DNA kit created from NH_2-modified SiO_2-coated Fe_3O_4 nanoparticles and highly fluorescent Mn-doped ZnS nanoparticles in a sandwich structure, which can be seen in Fig. 7.6. The sandwich configuration attached the fluorescent particles to the docking matrix of MNPs with the complementary hybridization of the detector probe−target−capture probe structure. In one side of this sandwich structure, SiO_2-coated Fe_3O_4 nanoparticles, which were modifed by the NH_2 group, were employed as a docking matrix. The docking matrix was linked with a capture probe oligonucleotide chain, which specifically identifies the target DNA. In the other side of the sandwich, the detector probe formed by the signaling semiconductor nanoparticles contacted with another oligonucleotide chain. This sandwich configuration was applied to detect DNA of EBV using separation function of MNPs and the signaling function of semmiconductor nanoparticles. The kit firstly was stored as three separated solutions containing magnetic probe nanoparticles, semiconductor detector nanoparticles, and target DNA molecules, respectively. In order to measure the target DNA concentration, those solutions

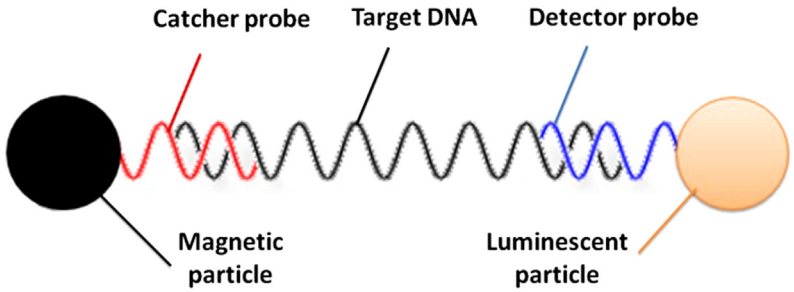

FIGURE 7.6

Schematic sandwich structure of DNA detection Fast kit using multifunctional magnetic–semiconductor nanoparticles.

After Quynh, L.M., Hieu, N.M., Nam, N.H., 2014. Fast DNA diagnostic using Fe_3O_4 magnetic nanoparticles and light emitting ZnS/Mn nanoparticles, VNU J. Sci.: Math. – Phys. 30(3), 1–11.

were mixed to assemble the magnetic donor–target DNA–semiconductor detector complexes via the specific hybridization of catcher probe and detector probe with the target DNA. The complexes, then, are easily collected by an outside magnetic field. The other components, which do not contain MNPs will be washed out. The collected complexes were redistributed in solution and measured by photoluminescence. The luminescent intensity at 586 nm of Mn-doped ZnS nanoparticles changes with changing the initially added DNA target concentration. The detection limit of target DNA is around 2×106 copies/mL (~ 0.3 fM), showing the ability of using the named multifunctional magnetic–semiconductor sandwich structure for fast KIT DNA detection during scene investigation and viral DNA detection.

Finally, in addition to the improved material properties, multifunctional materials are also important from an economic point of view. Multifunctional nanoparticle-based drug-delivery systems have been developed to improve the efficiency and reduce the systemic toxicity of a wide range of drugs, where additional capabilities like targeting and image contrast enhancement added to the nanoparticles. However, additional functionality means additional synthetic steps and costs, more convoluted behavior and effects in vivo, and also greater regulatory hurdles. The tradeoff between additional functionality and complexity is discussed by Cheng et al. (2012).

7.5 CONCLUSION AND PERSPECTIVES

This chapter reviews various methods of synthesis and functionalization of metallic, semiconductor, magnetic, and multifunctional nanoparticles. Some applications of the fabricated nanoparticles in life sciences and the environment are discussed.

In the synthesis domain, it is expected that new preparation approaches will be introduced allowing the use of less energy and less toxic materials ("green manufacturing"). In order to meet requirements for different applications, the functionality of nanoparticles becomes more complex. Thus the major trend in the further development of nanoparticles is to make them multifunctional, with the potential to integrate various functionalities. Smart multifunctional nanoparticles will be very promising for a variety of applications.

ACKNOWLEDGMENT

The authors would like to thank Prof. N.H. Hai, Prof. N.T.V. Anh, Prof. P.T. Nghia, Dr. P. Yen, Mr. L.M. Quynh, Dr. I. Notingher, and Prof. M. Henini for close collaboration.

REFERENCES

Akutsu, J.-I., Yuriko Tojo, Y., Segawa, O., Obata, K., Okochi, M., Tajima, H., et al., 2004. Development of an integrated automation system with a magnetic bead-mediated nucleic acid purification device for genetic analysis and gene manipulation. Biotechnol. Bioeng. 86, 667–671.

Alaqad, K., Saleh, T.A., 2016. Gold and silver nanoparticles: synthesis, methods, characterization routes and applications towards drugs. J. Environ. Anal. Toxicol. 6, 384.

Arruebo, M., Valladares, M., González-Fernández, A., 2009. Antibody-conjugated nanoparticles for biomedical applications. J. Nanomater. 2009, 439389.

Ashtari, P., He, X., Wang, K., Gong, P., 2005. An efficient method for recovery of target ssDNA based on amino-modified silica-coated magnetic nanoparticles. Talanta 67, 548–554.

Astruc, D. (Ed.), 2008. Nanoparticles and Catalysis. Wiley-VCH Verlag GmbH & Co. KGaA, Weinheim.

Babes, L., Denizot, B., Tanguy, G., Le Jeune, J.J., Jallet, P., 1999. Synthesis of iron oxide nanoparticles used as MRI contrast agents: a parametric study. J. Colloid Interface Sci. 212, 474–482.

Balakrishnan, S., Bonder, M.J., Hadjipanayis, G.C., 2009. Particle size effect on phase and magnetic properties of polymer-coated magnetic nanoparticles. J. Magn. Magn. Mater. 321, 117–122.

Bao, G., Mitragotri, S., Tong, S., 2013. Multifunctional nanoparticles for drug delivery and molecular imaging. Annu. Rev. Biomed. Eng. 15, 253–282.

Baxter, J.M., Patel, A.N., Varma, S., 2012. Facial basal cell carcinoma. BMJ 345, e5342.

Berensmeier, S., 2006. Magnetic particles for the separation and purification of nucleic acids. Appl. Microbiol. Biotechnol. 73, 495–504.

Boom, R., Sol, C.J., Salimans, M.M., Jansen, C.L., Wertheim-van Dillen, P.M., van der Noordaa, J., 1990. Rapid and simple method for purification of nucleic acids. J. Clin. Microbiol. 28, 495–503.

Boutonnet, M., Kizling, J., Steniu, P., 1982. The preparation of monodisperse colloidal metal particles from microemulsions. Colloids Surf. 5, 209–225.

Bruce, I.J., Sen, T., 2005. Surface modification of magnetic nanoparticles with alkoxysilanes and their application in magnetic bioseparations. Langmuir 21, 7029−7035.

Buffat, Ph, Borel, J.-P., 1976. Size effect on the melting temperature of gold particles. Phys. Rev. A 13, 2287−2298.

Bui, H.V., Nguyen, H.N., Hoang, N.N., Truong, T.T., Pham, V.B., 2014. Optical and magnetic properties of Mn-doped ZnS nanoparticles synthesized by hydrothermal method. IEEE Trans. Mag. 50, 2400404.

Byrappa, K., Adschiri, T., 2007. Hydrothermal technology for nanotechnology. Prog. Cryst. Growth Character. Mater. 53, 117−166.

Cai, L., Wang, W., Yang, X.Y., Zhou, P., Tang, H.W., Rao, J., et al., 2014. Preparation of fluorescent-magnetic silica nanoprobes for recognition and separation of human lung cancer cells. Austin J. Anal. Pharm. Chem. 1, 1027.

Caruso, F., 2001. Nanoengineering of particles surfaces. Adv. Mater. 13, 11−22.

Casset, F., Roux, F., Mouchet, P., Bes, C., Chardes, T., Granier, C., et al., 2003. A peptide mimetic of an anti-CD4 monoclonal antibody by rational design. Biochem. Biophys. Res. Commun. 307, 198−205.

Chaudhuri, R.G., Paria, S., 2012. Core/shell nanoparticles: classes, properties, synthesis mechanisms, characterization, and applications. Chem. Rev. 112, 2373−2433.

Cheng, Z., Zaki, A., Hui, J.Z., Muzykantov, V.R., Tsourkas, A., 2012. Multifunctional nanoparticles: cost versus benefit of adding targeting and imaging capabilities. Science 338, 903−910.

Daniel, M.C., Astruc, D., 2004. Gold nanoparticles: assembly, supramolecular chemistry, quantum-size-related properties, and applications toward biology, catalysis, and nanotechnology. Chem. Rev. 104, 293−346.

De, M., Ghosh, P.S., Rotello, V.M., 2008. Applications of nanoparticles in biology. Adv. Mater. 20, 4225−4241.

Dresco, P.A., Zaitsev, V.S., Gambino, R.J., Chu, B., 1999. Preparation and properties of magnetite and polymer magnetite nanoparticles. Langmuir 15, 1945−1951.

Dung, C.T., Loc, N.Q., Huong, P.T., Duong, D.T.T., Hong, T.T., Quynh, L.M., et al., 2014. Combination of 4-ATP coated silver nanoparticles and magnetic Fe_3O_4 nanoparticles by inverse emulsion method. VNU J. Sci.: Math. − Phys. 30, 1−9.

Dung, C.T., Quynh, L.M., Linh, N.P., Nam, N.H., Luong, N.H., 2016. Synthesis of ZnS: Mn-Fe_3O_4 bifunctional nanoparticles by inverse microemulsion method. J. Sci.: Adv. Mater. Dev. 1, 200−203.

Dung, C.T., Doanh, S.C., Quynh, L.M., Hong, T.T., Quach, T.D., Kim, D.H., et al., 2017a. Synthesis of bifunctional Fe_3O_4@SiO_2-Ag magnetic−plasmonic nanoparticles by an ultrasound assisted chemical method. J. Electron. Mater. 46, 3646−3653.

Dung, C.T., Quynh, L.M., Hong, T.T., Nam, N.H., 2017b. Synthesis, magnetic properties and enhanced photoluminescence of Fe_3O_4-ZnO heterostructure multifunctional nanoparticles. VNU J. Sci.: Math. − Phys. 33 (1), 14−21.

Elechiguerra, J.L., Burt, J.L., Morones, J.R., Camacho-Bragado, A., Gao, X., Lara, H.H., et al., 2005. Interaction of silver nanoparticles with HIV-1. J. Nanobiotechnol. 3, 6.

Ellis, R.C., Zabrowarny, L.A., 1993. Safer staining method for acid fast bacilli. J. Clin. Pathol. 46, 559−560.

European Commission, 2010. Scientific Basis for the Definition of the Term "Nanomaterial" European Commission, Scientific Committee on Emerging and Newly Identified Health Risks (SCENHR). Brussels, Belgium. Available at: http://ec.europa.eu/health/scientific_committees/emerging/docs/scenihr_o_032.pdf (accessed 25.06.18.).

Eustis, S., El-Sayed, M.A., 2006. Why gold nanoparticles are more precious than pretty gold: noble metal surface plasmon resonance and its enhancement of the radiative and nonradiative properties of nanocrystals of different shapes. Chem. Soc. Rev. 35, 209–217.

Feltin, N., Pileni, M.P., 1997. New technique for synthesizing iron ferrite magnetic nanosized particles. Langmuir 13, 3927–3933.

Filipponi, L., Sutherland, D., 2010. Environment: application of nanotechnologies. Nanoyou Teachers Training Kit in Nanotechnologies, pp. 1–26.

Frens, G., 1972. Particle size and sol stability in metal colloids. Colloid Polym. Sci. 250, 736–741.

Frens, G., 1973. Controlled nucleation for the regulation of the particle size in monodisperse gold suspensions. Nat. Phys. Sci. 241, 20–22.

Giani, G., Fedi, S., Barbucci, R., 2012. Hybrid magnetic hydrogel: a potential system for controlled drug delivery by means of alternating magnetic field. Polymers 4, 1157–1169.

Gupta, A.K., Gupta, M., 2005. Synthesis and surface engineering of iron oxide nanoparticles for biomedical applications. Biomaterials 26, 3995–4021.

Hai, N.H., Chau, N., Luong, N.H., Anh, N.T.V., Nghia, P.T., 2008. Application of magnetite nanoparticles for water treatment and for DNA and cell separation. J. Korean Phys. Soc. 53, 1601–1606.

Han, S.-B., Song, Y.-J., Lee, J.-M., Kim, J.-Y., Kim, D.-H., Park, K.-W., 2009. Synthesis of platinum nanostructure using seeding method. Bull. Korean Chem. Soc. 30, 2362–2364.

Harries, M., Smith, I., 2002. The development and clinical use of trastuzumab (Herceptin). Endocr. Relat. Cancer 9, 75–85.

Hayashi, H., Hakuta, Y., 2010. Hydrothermal synthesis of metal oxide nanoparticles in supercritical water. Materials 3, 3794–3817.

Hieu, N.M., Nam, N.H., Huyen, N.T., Anh, N.T.V., Nghia, P.T., Khoa, N.B., et al., 2017. Synthesis of SiO_2-coated Fe_3O_4 nanoparticles using ultrasound and its application in DNA extraction from formalin-fixed paraffin-embedded human cancer tissues. J. Electron. Mater. 46, 3738–3747.

Hirsch, L.R., Jackson, J.B., Lee, A., Halas, N.J., West, J.L., 2003. A whole blood immunoassay using gold nanoshells. Anal. Chem. 75, 2377–2381.

Hoa, T.T.Q., The, N.D., Mcvitie, S., Nam, N.H., Vu, L.V., Canh, T.D., et al., 2011. Optical properties of Mn-doped ZnS semiconductor nanoclusters synthesized by a hydrothermal process. Opt. Mater. 33, 308–314.

Hu, H., Wang, Z., Pan, L., Zhao, S., Zhu, S., 2010. Ag-coated Fe_3O_4@SiO_2 three-ply composite microspheres: synthesis, characterization, and application in detecting melamine with their surface-enhanced Raman scattering. J. Phys. Chem. C 114, 7738–7742.

Ilovitsh, T., Danan, Y., Meir, R., Meiri, A., Zalevsky, Z., 2015. Cellular imaging using temporally flickering nanoparticles. Sci. Rep. 5, 8244.

Irzh, A., Perkaz, N., Gedanken, A., 2007. Microwave-assisted coating of PMMA beads by silver nanoparticles. Langmuir 23, 9891–9897.

ISO/TS 80004-2: Nanotechnologies – Vocabulary – Part 2: Nano-objects. International Organization for Standardization, 2015.

Jain, K.K., 2005. Nanotechnology-based drug delivery for cancer. Technol. Cancer Res. Treat. 4, 407–416.

Jaiswal, J.K., Mattoussi, H., Mauro, J.M., Simon, S.M., 2003. Long-term multiple color imaging of live cells using quantum dot bioconjugates. Nat. Biotechnol. 21, 47–51.

Jia, F., Liu, X., Li, L., Mallapragada, S., Narasimhan, B., Wang, Q., 2013. Multifunctional nanoparticles for targeted delivery of immune activating and cancer therapeutic agents. J. Control. Release 172, 1020–1034.

Kamat, P.V., Shanghavi, B., 1997. Interparticle electron transfer in metal/semiconductor composites. Picosecond dynamics of CdS-capped gold nanoclusters. J. Phys. Chem. B 101, 7675–7679.

Karele, S., Gosavi, S.W., Urban, J., Kullarni, S.K., 2006. Nanoshell particles: synthesis, properties and applications. Curr. Sci. 91, 1038–1052.

Khalil, M.I., 2015. Co-precipitation in aqueous solution synthesis of magnetite nanoparticles using iron(III) salts as precusors. Arab. J. Chem. 8, 279–284.

Khuat, N.T., Nguyen, V.T.A., Phan, T.N., Hoang, L.H., Thach, C.V., Hai, N.H., et al., 2008. Sorting $CD4^+$ T cells in blood by using magnetic nanoparticles coated with anti-CD4 antibody. J. Korean Phys. Soc. 53, 3832–3836.

Kim, J.H., Kuk, E., Yu, K.N., Kim, J.-H., Park, J.S., Lee, H.J., et al., 2007. Antimicrobial effects of silver nanoparticles. Nanomedicine 3, 95–101.

Kim, M., Son, W.S., Ahn, K.H., Kim, D.S., Lee, H.S., Lee, Y.W., 2014. Hydrothermal synthesis of metal nanoparticles using glycerol as a reducing agent. J. Supercrit. Fluids 90, 53–59.

Kolk, A.H., Schuitema, A.R., Kuijper, S., van Leeuwen, J., Hermans, P.W., van Embden, J.D., et al., 1992. Detection of *Mycobacterium tuberculosis* in clinical samples by using polymerase chain reaction and a nonradioactive detection system. J. Clin. Microbiol. 30, 2567–2575.

Kolk, A.H.J., Kox, L.F.F., van Leeuwen, J., Kuijper, S., Jansen, H.M., 1998. Clinical utility of the polymerase chain reaction in the diagnosis of extrapulmonary tuberculosis. Eur. Respir. J 11, 1222–1226.

Kong, K., Rowlands, C.J., Varma, S., Perkins, W., Leach, I.H., Koloydenko, A.A., et al., 2013. Diagnosis of tumors during tissue-conserving surgery with integrated autofluorescence and Raman scattering microscopy. Proc. Natl. Acad. Sci. U.S.A. 110, 15189–15194.

Kortan, A.R., Hull, R., Opila, R.L., Bawendi, M.G., Steigerwald, M.L., Carroll, P.J., et al., 1990. Nucleation and growth of CdSe on ZnS quantum crystallite seeds, and vice versa, in inverse micelle media. J. Am. Chem. Soc. 112, 1327–1332.

Kox, L.F., Rhienthong, D., Miranda, A.M., Udomsantisuk, N., Ellis, K., van Leeuwen, J., et al., 1994. A more reliable PCR for detection of *Mycobacterium tuberculosis* in clinical samples. J. Clin. Microbiol. 32, 672–678.

Laurent, S., Forge, D., Port, M., Roch, A., Robic, C., Elst, L.V., et al., 2008. Magnetic iron oxide nanoparticles: synthesis, stabilization, vectorization, physicochemical characterizations, and biological applications. Chem. Rev. 108, 2064–2110.

Leslie-Pelecky, D.L., Labhasetwar, V.D., Kraus, R.H., 2005. Nanobiomagnetics. In: Sellmayer, D.J., Skomski, R.S. (Eds.), Advanced Magnetic Nanostructures. Kluver, New York.

Liu, X., Chang, Z., Luo, L., Lei, X., Liu, J., Sun, X., 2012. Sea urchin-like Ag-α-Fe_2O_3 nanocomposite microspheres: synthesis and gas sensing applications. J. Mater. Chem. 22, 7232–7238.

Liu, X.M., Li, Y.S., 2009. One-step facile fabrication of Ag/γ-Fe_2O_3 composite microspheres. Mater. Sci. Eng. C 29, 1128–1132.

Liu, Z., Zhao, B., Shi, Y., Guo, C., Yang, H., Li, Z., 2010. Novel nonenzymatic hydrogen peroxide sensor based on iron oxide-silver hybrid submicrospheres. Talanta 81, 1650–1654.

Loo, C., Lin, A., Hirsch, L., Lee, M.H., Barton, J., Halas, N., et al., 2004. Nanoshell-enabled photonics-based imaging and therapy of cancer. Technol. Cancer Res. Treat. 3, 33–40.

Lopez-Quintela, M.A., Rivas, J., 1993. Chemical reactions in microemulsions: a powerful method to obtain ultrafine particles. J. Colloid Interface Sci. 158, 446–451.

Lu, A.-H., Salabas, E.L., Schuth, F., 2007. Magnetic nanoparticles: synthesis, protection, functionalization, and application. Angew. Chem. Int. Ed. 46, 1222–1244.

Luong, N.H., Hai, N.H., Phu, N.D., MacLaren, D.A., 2011. Co-Pt nanoparticles encapsulated in carbon cages prepared by sonoelectrodeposition. Nanotechnology 22, 285603.

Mascolo, M.C., Pei, Y., Ring, T.A., 2013. Room temperature co-precipitation synthesis of magnetite nanoparticles in a large pH window with different bases. Materials 6, 5549–5567.

Melaine, F., Roupioz, Y., Buhot, A., 2015. Gold nanoparticles surface plasmon resonance enhanced signal for the detection of small molecules on split-aptamer microarrays (small molecules detection from split-aptamers). Microarrays 4, 41–52.

Mews, A., Eychmueller, A., Giersig, M., Schooss, D., Weller, H., 1994. Preparation, characterization, and photophysics of the quantum dot quantum well system CdS/HgS/CdS. J. Phys. Chem. 98, 934–941.

Michalet, X., Pinaud, F.F., Bentolila, L.A., Tasy, J.M., Doose, S., Li, J.J., et al., 2005. Quantum dots for live cells, in vivo imaging, and diagnostics. Science 307, 538–544.

Mohan, S.V., Chang, A.L., 2014. Advanced basal cell carcinoma: epidemiology and therapeutic innovations. Curr. Dematol. Rep. 3, 40–45.

Mody, V.V., Siwale, R., Singh, A., Mody, H.R., 2010. Introduction to metallic nanoparticles. J. Pharm. Bioallied Sci. 2, 282–289.

Nam, N.H., Van, N.T.T., Phu, N.D., Hong, T.T., Hai, N.H., Luong, N.H., 2012. Magnetic properties of FePt nanoparticles prepared by sonoelectrodeposition. J. Nanomater. 2012, 801240.

National Cancer Intelligence Network (NCIN), 2013. Non-Melanoma Skin Cancer in England, Scotland, Northern Ireland, and Ireland. NCIN, London.

Nguyen, D.Q., Duong, P.T., Nguyen, H.M., Nam, N.H., Luong, N.H., Pham, Y., 2016. New biological treatment targeting *Mycobacterium tuberculosis* in contaminated wastewater using lysing enzymes coupled to magnetic nanoparticles. Green Process Synth. 5, 473–478.

Nguyen, H.L., Nguyen, H.N., Nguyen, H.H., Luu, M.Q., Nguyen, M.H., 2015. Nanoparticles: synthesis and applications in life science and environmental technology. Adv. Nat. Sci.: Nanosci. Nanotechnol. 6, 015008.

Noordhoek, G.T., Kolk, A.H., Bjune, G., Catty, D., Dale, J.W., Fine, P.E., et al., 1994. Sensitivity and specificity of PCR for detection of *Mycobacterium tuberculosis*: a blind comparison study among seven laboratories. J. Clin. Microbiol. 32, 277–284.

Ogbaini-Emovon, O., 2009. Current trends in the laboratory diagnosis of Tuberculosis. Benin J. Postgrad. Med. 11 (No. 1; Supplemental Issue), 79–90.

Okoye, A.A., Picker, L.J., 2013. CD4 + T-cell depletion in HIV infection: mechanisms of immunological failure. Immunol. Rev. 254, 54–64.

Oldenburg, S.J., Averitt, R.D., Westcott, S.L., Halas, N.J., 1998. Nanoengineering of optical resonances. Chem. Phys. Lett. 288, 243–247.

Paciotti, G.F., Myer, L., Weinreich, D., Goia, D., Pavel, N., McLaughlin, R.E., et al., 2004. Colloidal gold: a novel nanoparticle vector for tumor directed drug delivery. Drug Deliv. 11, 169–183.

Pal, S., Tak, Y.K., Song, J.M., 2007. Does the antibacterial activity of silver nanoparticles depend on the shape of the nanoparticle? A study of the gram-negative bacterium *Escherichia coli*. Appl. Environ. Microbiol. 73, 1712–1720.

Patnaik, P., 2004. Dean's Analytical Chemistry Handbook, second ed. McGraw-Hill.

Perrault, S.D., Chan, W.C.W., 2009. Synthesis and surface modification of highly monodispersed, spherical gold nanoparticles of 50–200 nm. J. Am. Chem. Soc. 131, 17042–17043.

Phadtare, S., Kumar, A., Vinod, V.P., Dash, C., Palaskar, D.V., Rao, M., et al., 2003. Direct assembly of gold nanoparticle "shells" on polyurethane microsphere "cores" and their applications as enzyme immobilization templates. Chem. Mater. 15, 1944–1949.

Pham, Y., Nguyen, A.T.V., Phan, T.-N., Chu, L.L., Nguyen, D.Q., Nguyen, H.M., et al., 2015. Specificity and processing rate enhancement of *Mycobacterium tuberculosis* diagnostic procedure using antibody-coupled magnetic nanoparticles. Int. J. Nanotechnol. 12 (5/6/7), 335–346.

Qi, L., Ma, J., Cheng, H., Zhao, Z., 1996. Synthesis and characterization of mixed CdS/ZnS nanoparticles in reverse micelles. Colloids Surf. A 111, 195–202.

Quy, D.V., Hieu, N.M., Tra, P.T., Nam, N.H., Hai, N.H., Son, N.T., et al., 2013. Synthesis of silica-coated magnetic nanoparticles and application in the detection of pathogenic viruses. J. Nanomater. 2013, 603940.

Quynh, L.M., Tuan, T.Q., Luong, N.H., Long, N.N., Hai, N.H., Thoa, T.T.T., et al., 2011. Application of gold nanoparticles for early detection of breast cancer cells. e-J. Surf. Sci. Nanotech 9, 544–547.

Quynh, L.M., Hieu, N.M., Nam, N.H., 2014. Fast DNA diagnostic using Fe_3O_4 magnetic nanoparticles and light emitting ZnS/Mn nanoparticles. VNU J. Sci.: Math. – Phys 30 (3), 1–11.

Quynh, L.M., Nam, N.H., Kong, K., Nhung, N.T., Notinger, I., Henini, M., et al., 2016. Surface-enhanced Raman spectroscopy study of 4-ATP on gold nanoparticles for basal cell carcinoma fingerprint detection. J. Electron. Mater. 45, 2563–2568.

Rioux, D., Meunier, M., 2015. Seeded growth synthesis of composition and size-controlled gold-silver alloy nanoparticles. J. Phys. Chem. C 119, 13160–13168.

Ryan, K.J., Ray, C.G. (Eds.), 2004. Sherris Medical Microbiology. fourth ed. McGraw Hill, New York.

Salata, O.V., 2004. Applications of nanoparticles in biology and medicine. J. Nanobiotechnol. 2, 3.

Salgueirino-Maceira, V., Correa-Duarte, M.A., 2007. Increasing the complexity of magnetic core/shell structured nanocomposites for biological application. Adv. Mater. 19, 4131–4144.

Sankar, S., Kuppanan, S., Balakrishnan, B., Nandagopal, B., 2011. Analysis of sequence diversity among IS6110 sequence of *Mycobacterium tuberculosis*: possible implications for PCR based detection. Bioinformation 6, 283–285.

Scodeller, P., Flexer, V., Szamocki, R., Calvo, E.J., Tognalli, N., Troiani, H., et al., 2008. Wired-enzyme core-shell Au nanoparticle biosensor. J. Am. Chem. Soc. 130, 12690–12697.

Sedaghat, S., Nasseri, A., 2011. Synthesis and stabilization of Ag nanoparticles on a polyamide (nylon 6,6) surface and its antibacterial effects. Int. Nano Lett. 1, 22–24.

Seleci, M., Seleci, D.A., Joncyzk, R., Stahl, F., Blume, C., Scheper, T., 2016. Smart multifunctional nanoparticles in nanomedicine. BioNanoMat 17, 33–41.

Sewage water treatment vat. Available from: <https://microbewiki.kenyon.edu/index.php/Sewage_Water_Treatment_Vat#Harmful_Bacteria>. (accessed January 2016).

Sharma, G., Jeevanandam, P., 2013. A facile synthesis of multifunctional iron oxide@Ag core−shell nanoparticles and their catalytic applications. Eur. J. Inorg. Chem. 2013, 6126−6136.

Sharma, V.K., Yngard, R.A., Lin, Y., 2009. Silver nanoparticles: green synthesis and their antimicrobial activities. Adv. Colloid Interface Sci. 145, 83−96.

Shenava Aashritha, 2013. Synthesis of silver nanoparticles by chemical reduction method and their antifungal activity. Int. Res. J. Pharm. 4, 111−113.

Shi, B., Shin, Y.K., Hassanali, A.A., Singer, S., 2015. DNA binding to the silica surface. J. Phys. Chem. B 119, 11030−11040.

Shukla, I., Varshney, S., Sarfraz, Malik, A., Ahmad, Z., 2011. Evaluation of nested PCR targeting IS6110 of *Mycobacterium tuberculosis* for the diagnosis of pulmonary and extra-pulmonary tuberculosis. Biol. Med. 3, 171−175.

Sokolov, K., Follen, M., Aaron, J., Pavlova, I., Malpica, A., Lotan, R., et al., 2003. Real-time vital optical imaging of precancer using anti-epidermal growth factor receptor antibodies conjugated to gold nanoparticles. Cancer Res. 63, 1999−2004.

Sondi, I., Salopek-Sondi, B., 2004. Silver nanoparticles as antimicrobial agent: a case study on *E. coli* as a model for Gram-negative bacteria. J. Colloid Interface Sci 275, 177−182.

Sotiriou, G.A., Hirt, A.M., Lozach, P.Y., Teleki, A., Krumeich, F., Pratsinis, S.E., 2011. Hybrid, silica-coated, Janus-like plasmonic-magnetic nanoparticles. Chem. Mater. 23, 1985−1992.

Sparnacci, K., Laus, M., Tondelli, L., Magnani, L., Bernardi, C., 2002. Core-shell microspheres by dispersion polymerization as drug delivery systems. Macromol. Chem. Phys. 203, 1364−1369.

Subbiah, R., Veerapandian, M., Yun, K.S., 2010. Nanoparticles: functionalization and multifunctional applications in biomedical sciences. Curr. Med. Chem. 17, 4559−4577.

Sun, C., Sze, R., Zhang, M., 2006. Folic acid-PEG conjugated superparamagnetic nanoparticles for targeted cellular uptake and detection by MRI. J. Biomed. Mater. Res. Part A 78 (3), 550−557.

Sun, Y., Tian, Y., He, M., Zhao, Q., Chen, C., Hu, C., et al., 2012. Controlled synthesis of Fe_3O_4/Ag core-shell composite nanoparticles with high electrical conductivity. J. Electron. Mater. 41, 519−523.

Takamori, S., Kong, K., Varma, S., Leach, I., Williams, H.C., Notingher, I., 2015. Optimization of multimodal spectral imaging for assessment of resection margins during Mohs micrographic surgery for basal cell carcinoma. Biomed. Opt. Express 6, 98−111.

Tuan, M.A., Binh, N.H., Tam, P.D., Chien, N.D., 2005. Conductometric biosensor for diabetic diagnosis and DNA detection in transgenic corn. Comm. Phys 15, 218−222.

Tuan, T.Q., Son, N.V., Dung, H.T.K., Luong, N.H., Thuy, B.T., Anh, N.T.V., et al., 2011. Preparation and properties of silver nanoparticles loaded in activated carbon for biological and environmental applications. J. Hazard. Mater. 192, 1321−1329.

Ulman, A., 1996. Formation and structure of self-assembled monolayers. Chem. Rev. 96, 1533−1554.

West, J.L., Halas, N.J., 2000. Application of nanotechnology to biotechnology: Commentary. Curr. Opin. Biotechnol. 11, 215−217.

Williams, J.V., Adams, C.N., Kotov, N.A., Savage, P.E., 2007. Hydrothermal synthesis of CdSe nanoparticles. Ind. Eng. Chem. Res. 46, 4358−4362.

World Health Organization, 2007. WHO Case Definitions of HIV for Surveillance and Revised Clinical Staging and Immunological Classification of HIV-Related Disease in Adults and Children. Geneva.

World Health Organization, 2011. Global Tuberculosis Control, WHO library.

Xu, Z.-C., Shen, C.-M., Xiao, C.-W., Yang, T.-Z., Zhang, H.-R., Li, J.-Q., et al., 2007. Wet chemical synthesis of gold nanoparticles using silver seeds: a shape control from nanorods to hollow spherical nanoparticles. Nanotechnology 18, 115608.

Yan, E., Ding, Y., Chen, C., Li, R., Hu, Y., Jiang, X., 2009. Polymer/silica hybrid hollow nanospheres with pH-sensitive drug release in physiological and intracellular environments. Chem. Commun. 2009, 2718–2720.

Yezhelyev, M.V., Gao, X., Xing, Y., Al-Hajj, A., Nie, S., O'Regan, R.M., 2006. Emerging use of nanoparticles in diagnosis and treatment of breast cancer. Lancet Oncol. 7, 657–667.

Zhang, L., Gu, F.X., Chan, J.M., Wang, A.Z., Langer, R.S., Farokhzad, O.C., 2008. Nanoparticles in medicine: therapeutic applications and developments. Clin. Pharmacol. Ther. 83, 761–769.

Zhu, J., Liu, S., Palchik, O., Koltypin, Y., Gedanken, A., 2000. Shape-controlled synthesis of silver nanoparticles by pulse sonoelectrochemical methods. Langmuir 16, 6396–6399.

Ziegler, C., Eychmuller, A., 2011. Seeded growth synthesis of uniform gold nanoparticles with diameters of 15-300 nm. J. Phys. Chem. C 115, 4502–4506.